THE JOURNAL OF
PHYSICAL CHEMISTRY C

ARTICLE

pubs.acs.org/JPCC

Elementary Steps, the Role of Chemisorbed Oxygen, and the Effects of Cluster Size in Catalytic CH_4-O_2 Reactions on Palladium

Ya-Huei (Cathy) Chin and Enrique Iglesia*

Department of Chemical and Biomolecular Engineering, University of California, Berkeley, California 94720, United States

S Supporting Information

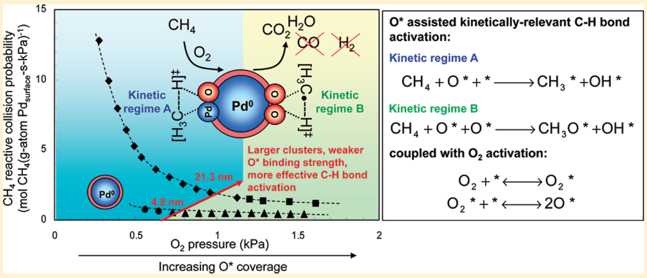

ABSTRACT: Kinetic and isotopic data and effects of cluster size are used to probe elementary steps and their kinetic relevance in CH_4-O_2 reactions on Pd clusters that retain a metallic bulk during catalysis. CO_2 and H_2O were the only products detected, except when O_2 was nearly depleted, during which trace CO amounts were formed. $^{13}CH_4-^{12}CO-O_2$ reactions showed that CO reacts with chemisorbed oxygen (O*) much faster than CH_4 with reactive collision probability ratios for CO and CH_4 proportional to O_2/CO ratios via a constant exceeding 500. Thus, even if CO desorbed before forming CO_2, it would oxidize via reactions with O* at any reactor residence time required for detectable CH_4 conversion, making direct partial oxidation impractical as a molecular route to H_2-CO mixtures on Pd. CH_4 turnover rates and effective first-order rate constants initially decreased and then reached constant values as O_2 pressure and O* coverage increased as a result of a transition in the surface species involved in kinetically relevant C−H bond activation steps from O*−* to O*−O* site pairs (*, vacancy site). On O*−O* site pairs, C−H bonds are cleaved via H-abstraction mediated by O* and radical-like CH_3 fragments weakly stabilized by the vicinal O* are formed at the transition state. These reactions show large activation barriers (158 kJ mol^{-1}) but involve high entropy transition states that lead to larger pre-exponential factors (1.48×10^9 kPa^{-1} s^{-1}) than for tighter transition states involved in C−H bond activation by *−* site pairs for CH_4 reactions with H_2O or CO_2 (barriers: 82.5 kJ mol^{-1} and pre-exponential factors: 3.5×10^5 kPa^{-1} s^{-1}). CH_3 fragments at the transition state are effectively stabilized by interactions with vacancy sites on O*−* site pairs, which lead to higher turnover rates, as vacancies become available with decreasing O_2 pressure. CH_4-O_2 turnover rates and C−H bond activation rate constants on O*−O* site pairs decreased with decreasing Pd cluster size, because coordinatively unsaturated exposed atoms on small clusters bind O* more strongly and decrease its reactivity for H-abstraction. The stronger O* binding on small Pd clusters also causes the kinetic involvement of O*−* sites to become evident at lower O_2 pressures than on large clusters. These effects of metal−oxygen bond strength on O* reactivity also lead to the smaller turnover rates observed on Pd clusters compared with Pt clusters of similar size. These effects of cluster size and metal identity and their O* binding energy are the root cause for reactivity differences and appear to be general for reactions involving vacancies in kinetically relevant steps, as is the case for CH_4, C_2H_6, NO, and CH_3OCH_3 oxidation on O*-covered surfaces and for hydrogenation of organosulfur compounds on surfaces nearly saturated with chemisorbed sulfur.

1. INTRODUCTION

Small Pd clusters dispersed on high surface area substrates are useful as CH_4 combustion catalysts in power generation and exhaust gas treatment.[1−4] Similar catalysts also promote CH_4-O_2 reactions at substoichiometric ratios ($O_2/CH_4 < 2$) to form CO and H_2 via mildly exothermic routes.[5] The latter reactions produce synthesis gas or H_2 via less endothermic routes than CH_4-H_2O/CO_2 reforming (ΔH°_{298} = 206 kJ mol^{-1} (H_2O), 247 kJ mol^{-1} (CO_2))[6,7] and lessen heat transfer requirements and catalyst deactivation. Autothermal reformers use O_2 in flame combustion of CH_4 in $CH_4-H_2O-O_2$ mixtures at the reactor inlet to provide the heat required for subsequent reforming reactions.[8] These autothermal routes lead to sharp temperature profiles along the catalyst bed, which would be absent if direct catalytic partial oxidation occurred at the molecular scale or within thermal conduction distances in monoliths or packed bed reactors.

The reactions that form CO_2-H_2O[9−11] and $CO-H_2$[7,12−14] from CH_4-O_2 reactants on Pd have been previously examined, but the required active sites, the detailed sequence of the elementary steps, and their kinetic relevance and even whether H_2 and CO can form directly as primary products remain issues of active debate and considerable controversy. These issues reflect, at least in part, the presence of ubiquitous temperature and concentration gradients within catalyst pellets and beds as a result of the fast nature of these reactions, the typical high conversions that prevail, and the highly exothermic nature of combustion reactions (ΔH°_{298}= −802 kJ mol^{-1}). The chemical transformations between Pd and PdO bulk chemical states also complicate the mechanistic interpretation of concentration and temperature

Received: April 9, 2011
Revised: July 18, 2011
Published: July 21, 2011

dx.doi.org/10.1021/jp203324y | J. Phys. Chem. C 2011, 115, 17845−17855

effects on rate data in terms of elementary steps and their kinetic relevance. These metal-oxide transformations occur in response to changes in oxygen chemical potential and temperature[15−17] as O_2 is depleted along the reactor or within porous catalyst pellets. These changes in chemical state can occur concurrently with structural transformations that alter the shape of such clusters and the intimacy of their contact with supports, which alter, in turn, the coverage and reactivity of oxygen atoms, as shown when surfaces of Pd foil interconvert between metal and oxide states.[18]

Here we provide evidence of the chemical origins of the rate and selectivity observed in CH_4-O_2 reactions on Pd clusters by measuring the rate of chemical events in the absence of transport corruptions in a range of oxygen chemical potentials that maintains the bulk of Pd clusters (4.5−22.3 nm) in their metallic state. Our recent studies in CH_4-O_2 reactions on Pt[19,20] and CH_4-H_2O/CO_2[21−27] reactions on several metals (Rh,[21] Pt,[22] Ir,[24,25] Ni,[26] Ru,[23] and Pd[27]) have probed the elementary steps and site requirements for these reactions. CH_4-H_2O/CO_2 turnover rates on Pd clusters are limited by C−H bond activation steps on *−* site pairs,[27] as also found on other metals,[21−24,26] but rate constants are significantly larger than those on other metals and cause C−H bond dissociation to become reversible. Fast C−H bond activation on Pd also leads to kinetically detectable coverages by C* and H* intermediates, which inhibit reforming reactions.[27] In CH_4-O_2 mixtures, O*−* and O*−O* site pairs on Pt cluster surfaces activate C−H bonds with different activation enthalpies and entropies, kinetic dependencies, and cluster size effects than the *−* site pairs that activate CH_4 in reactions with H_2O/CO_2.[19] These concepts are extended here to Pd clusters, for which elementary steps and their kinetic relevance for CH_4-O_2 reactions and the selectivity of chemisorbed oxygen in reactions with CH_4 and CO remain uncertain.

We address the catalytic consequences of using O_2 as the oxidant and the role of chemisorbed oxygen (O*) in CH_4-O_2 reactions on metallic Pd clusters by measuring reaction rates and selectivities in kinetic control regime without transport artifacts. The chemical equilibrium between O* species and O_2(g) was confirmed by $^{16}O_2-^{18}O_2$ isotopic exchange probe reactions. In a parallel study, we address the behavior of CH_4-O_2 reactions on PdO clusters[28] and the dynamics of Pd−PdO phase transition.[29] Kinetic and isotopic studies are used to determine the role of O* in the kinetically relevant elementary steps for CH_4-O_2 reactions and to establish that CO does not form at detectable levels during these reactions on Pd clusters. $^{13}CH_4-CO-O_2$ reactions showed that even if CO* desorbed unreacted, it would react with O* at any residence time required for detectable CH_4 conversion, indicating that direct partial oxidation is not feasible on Pd clusters and that CO (and H_2) form exclusively via sequential reforming reactions. The proposed sequence of elementary steps is consistent with rate data, CH_4/CD_4 kinetic isotope effects, oxygen exchange kinetics, and with steps that mediate CH_4-H_2O/CO_2 reactions on group VIII metals[21−24,26] and CH_4-O_2 reactions on Pt.[19,20] Kinetically relevant C−H bond activation steps occur on O*−O* site pairs at O*-saturated surfaces and on O*−* site pairs as O* coverages decrease below saturation. Rate constants for C−H bond activation increased with increasing Pd cluster size as a result of a concomitant decrease in O* binding energy. These kinetically relevant steps and active site structures were similar to those proposed for Pt; the rate constants were, however, smaller because O* binding is stronger on Pd than Pt clusters of similar size.

2. EXPERIMENTAL METHODS

2.1. Synthesis of Dispersed Pd Clusters on High Surface Area Oxide Supports. $\gamma-Al_2O_3$ (Sasol North America, lot no. C1643, 193 $m^2\ g^{-1}$, 0.57 $cm^3\ g^{-1}$ pore volume) and SiO_2 (Davison Chemical, grade 923, CAS no. 112926-00-8, 280 $m^2\ g^{-1}$, 0.85 $cm^3\ g^{-1}$ pore volume) supports were treated in flowing dry air (Praxair, zero grade, 0.083 K s^{-1}, 60 $cm^3\ g^{-1}$) at 923−1073 K for 5 h before impregnation with aqueous $Pd(NO_3)_2$ solutions (Aldrich, 99.999% purity, 10 wt % $Pd(NO_3)_2$ in 10 wt % HNO_3) to obtain samples containing 0.2 wt % Pd. Impregnated samples were treated in stagnant ambient air at 383 K for 8 h and then in flowing dry air (Praxair, zero grade, 60 $cm^3\ g^{-1}$) by heating to 623 at 0.033 K s^{-1} (3 h hold) and then to 923−1073 K at 0.083 K s^{-1} (5 h hold) and cooling to ambient temperature. A portion of the catalysts was then treated in flowing H_2−Ar mixture (10% H_2/Ar, 0.083 K s^{-1}, 60 $cm^3\ g^{-1}$, Praxair certified standard) at a temperature between 923 and 1023 K for 3 h, cooled to 673 K, and then treated in He (Praxair UHP grade, 60 $cm^3\ g^{-1}$) at 673 K before cooling to ambient temperature. O_2/He mixtures (0.5% O_2/He, Praxair certified standard, 60 $cm^3\ g^{-1}$) were introduced to the samples at ambient temperature for at least 2 h before exposure to ambient air. The fraction of exposed Pd atoms was determined by volumetric O_2 chemisorption experiments carried out on a Quantachrome Autosorb-1 unit at 313 K. The number of exposed Pd atoms was determined from extrapolation of O_2 adsorption isotherm to zero pressure with the assumption that the atomic ratio of oxygen-to-exposed Pd equals one and Pd clusters are in hemispherical shapes with a metal density of bulk Pd (12.0 g cm^{-3}).[30]

2.2. Measurements of CH_4-O_2 Turnover Rates and O_2 Selectivities. Steady-state CH_4 conversion turnover rates were measured at 873−973 K in a tubular flow reactor (quartz; 8.1 mm inner diameter) with plug flow hydrodynamics. Catalysts were diluted with inert SiO_2 (Davison Chemical, Chromatographic Silica Media, CAS no. 112926-00-8, 280 $m^2\ g^{-1}$) at a diluent-to-catalyst mass ratio of 50−200, pelletized, and sieved to retain 106−250 μm aggregates. These particles were then mixed with quartz (Fluka, acid purified, product number 84880, 106−250 μm diameters) at a diluent-to-Pd/Al_2O_3 catalyst mass ratio in the range of 150−450.

Catalyst samples were heated to reaction temperatures in a flowing H_2−He mixture (5 kPa H_2 in He, Praxair, UHP grade, 0.083 K s^{-1}, 1.67 $cm^3\ s^{-1}$) and then treated in He (Praxair UHP grade, 1.67 $cm^3\ s^{-1}$) for ~0.2 h. Reactant mixtures consisting of 25% CH_4/He (Matheson, Certified Plus grade), 1% CO/He (Praxair, Certified Standard), O_2 (Praxair, UHP) or 5% O_2/He (Praxair, Certified Standard), and He (Praxair, UHP grade) were metered using electronic mass flow controllers (Porter 201). H_2O (doubly distilled and deionized) or D_2O (Aldrich, 99.9% D) were introduced using a syringe (Hamilton, no. 1005, 5000 μL) at a rate controlled by a syringe pump (Cole Parmer, model 60061) into a heated line (423 K) swept by gaseous reactants. Reactant and product concentrations were measured using a gas chromatograph (Agilent 3000A Micro GC) equipped with modules that contain Poraplot Q or Mol Sieve 5A columns and thermal conductivity detectors. The reactor was operated in a differential mode, where CH_4 conversions were maintained below 4% and for kinetic measurements in Section 3.5 below 0.5%. CH_4 turnover rates were determined from effluent CO and CO_2 concentrations and O_2 chemisorption uptakes, the latter of which provides the total number of exposed Pd atoms available for chemical turnovers.

Reactions of $^{16}O_2-^{18}O_2$, $CH_4-^{16}O_2-^{18}O_2$, $^{13}CH_4-^{12}CO-O_2$, CD_4-O_2, $^{13}CH_4-^{12}CO_2-O_2$, $CD_4-H_2O-O_2$, and $CH_4-D_2O-O_2$ mixtures were carried out in the tubular flow reactor described above by incorporating isotopic compounds (2% $^{18}O_2$/He (Icon, 98% ^{18}O), $^{13}CH_4$ (Isotec, 99% ^{13}C), CD_4 (Isotec, 99% D), or D_2O (Sigma-Aldrich, >99.9% D)) into the feed mixtures. The isotopic composition of each chemical species in inlet and outlet streams was measured by mass spectrometry (Agilent 6890 and 5973 N). $CaSO_4$ (Drierite) was used to remove water isotopologues before analysis.

Table 1. Intrapellet and Bed Dilution Effects on CH_4 Combustion Turnover Rates on a 0.2 wt % Pd/Al_2O_3 (21.3 nm Mean Pd Cluster Diameter) Catalyst at 973 K

catalyst mass (mg)	intrapellet dilution ratio (SiO_2/catalyst)[a]	bed dilution ratio (quartz/catalyst)[a]	turnover rate (mol CH_4 (g-atom $Pd_{surface}$ s)$^{-1}$)[b]
2.0	50	150	37
1.0	50	280	35
2.5	200	280	41

[a] Mass ratio of diluent-to-Pd/Al_2O_3 catalyst. [b] 4.86 kPa CH_4, 1.54 kPa O_2, 2.08 cm^3 s^{-1}, time-on-stream = 3.6 ks.

3. RESULTS AND DISCUSSION

3.1. Effects of Intrapellet and Bed Dilution on CH_4 Conversion Turnover Rates.

Reactions of CH_4 with O_2 on supported Pd clusters form CO_2 and H_2O almost exclusively at all conditions leading to detectable outlet O_2 concentrations (Section 3.2). Sequential reactions of CH_4 with CO_2 and H_2O combustion products form CO (and H_2) after O_2 depletion. Prevalent exothermic combustion reactions cause severe temperature and concentration gradients within individual catalyst pellets and across the reactor bed in the absence of extensive dilution at the bed and pellet scales, which allows rates to be measured under conditions of strict kinetic control.[31,32] Measured CH_4

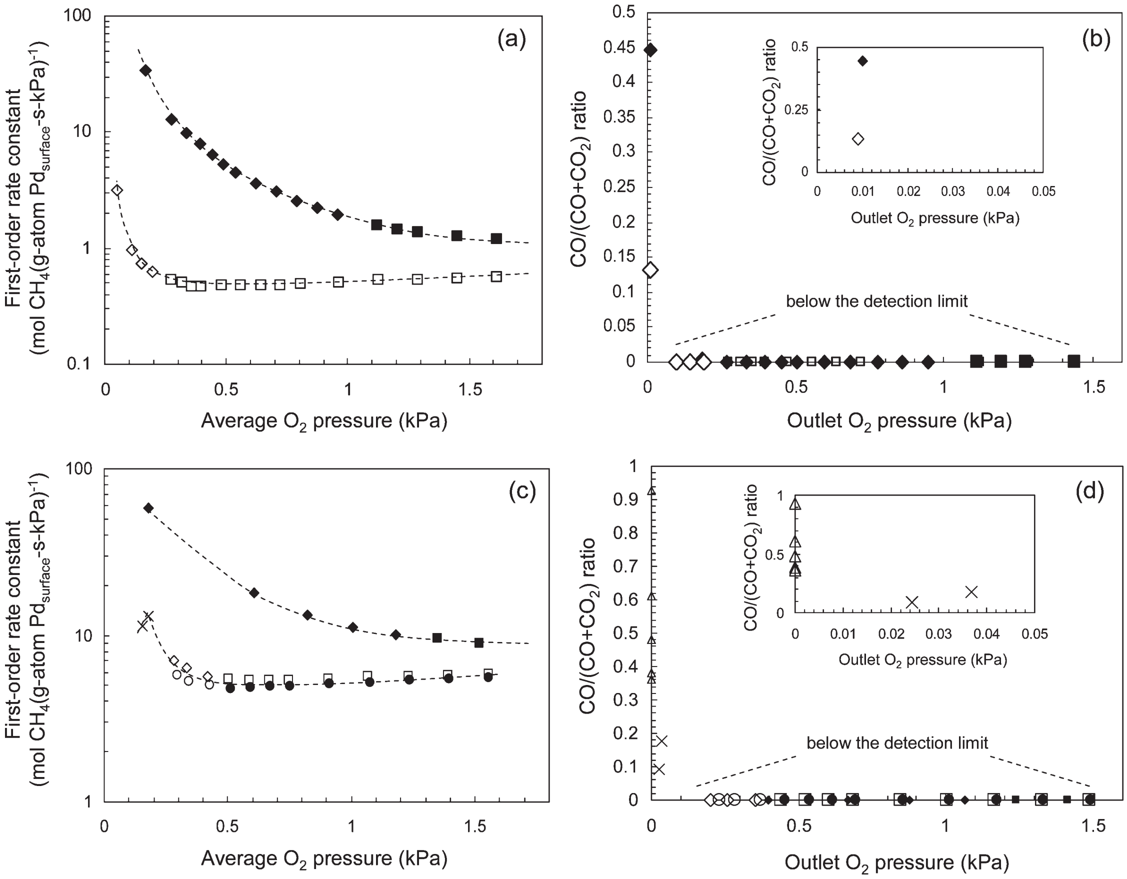

Figure 1. (a) O_2 pressure dependence of first-order rate constants ($r_{CH_4}(CH_4)^{-1}$, also the reactive CH_4 collision probabilities) during CH_4-O_2 reactions at 873 K and time-on-stream intervals of 0−7.2 (◆,■) and 59.4−63 ks (◇,□) on a 0.2 wt % Pd/Al_2O_3 catalyst (21.3 nm mean Pd cluster diameter). Two distinct kinetic regimes are observed, where the rate constants are inversely proportional to (◆,◇) and independent of (■,□) O_2 pressure, respectively. (b) Effects of outlet O_2 pressure on fractional CO contents, $CO/(CO + CO_2)$, during CH_4-O_2 reactions at 873 K and time-on-stream intervals of 0−7.2 ks (◆,■) and 59.4−63 ks (◇,□) on a 0.2 wt % Pd/Al_2O_3 catalyst (21.3 nm mean Pd cluster diameter). Inset: region of low outlet O_2 pressure of 0 to 0.05 kPa. (c) O_2 pressure dependence of first-order rate constants ($r_{CH_4}(CH_4)^{-1}$, also the reactive CH_4 collision probabilities) during CH_4-O_2 reactions at 973 K and time-on-stream intervals of 0−7.2 ks (◆,■), 32.4−38.0 ks (◇,□), and 77.4−82.8 ks (×,○,●) on 0.2 wt % Pd/Al_2O_3 catalyst (21.3 nm mean Pd cluster diameter). Three distinct kinetic regimes are observed, where the rate constants are proportional to (×), inversely proportional to (◆,◇,○) and independent of (■,□,●) O_2 pressure. (d) Effects of outlet O_2 pressure on fractional CO contents, $CO/(CO + CO_2)$, during CH_4-O_2 reactions at 973 K and time-on-stream intervals of 0−7.2 ks (◆,■), 32.4−38.0 ks (◇,□), and 77.4−82.8 ks (×,○,●) on 0.2 wt % Pd/Al_2O_3 catalyst (21.3 nm mean Pd cluster diameter). Additional data on the fractional CO contents after O_2 depletion (△) are also included here. Inset: region of low outlet O_2 pressure of 0 to 0.05 kPa.(4.85 kPa CH_4, 1.57 × 10^9 cm^3 (s g-atom $Pd_{surface}$)$^{-1}$, 200 SiO_2/catalyst intraparticle dilution ratio, 450 quartz/catalyst bed dilution ratio).

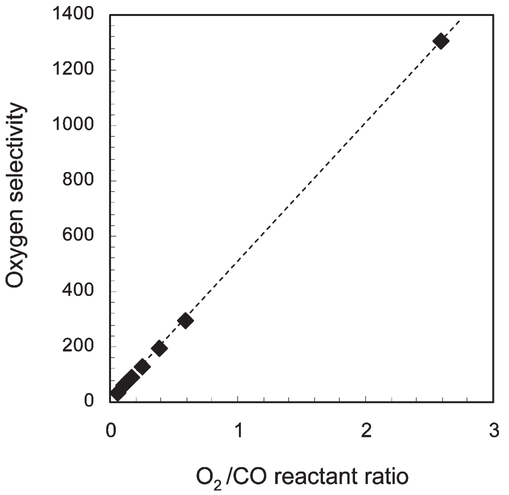

Figure 2. O_2/CO reactant ratio effects on oxygen selectivity, defined as the ratio of first-order rate constants (also the reactive collision probabilities) for CO and CH_4 oxidation (eq 1) during $^{13}CH_4$–^{12}CO–O_2 reactions on a 0.2 wt % Pd/Al_2O_3 (21.3 nm mean Pd cluster diameter) catalyst at 973 K (4.85 kPa $^{13}CH_4$, 0.81 kPa ^{12}CO, 0.081 to 0.36 kPa O_2, 1.57×10^9 cm^3 (s g-atom $Pd_{surface}$)$^{-1}$, 200 SiO_2/catalyst intraparticle dilution ratio, 450 quartz/catalyst bed dilution ratio).

combustion turnover rates (Table 1, per exposed Pd atom; 973 K) on 0.2 wt % Pd/Al_2O_3 (21.3 nm mean Pd cluster diameter) were identical within the experimental errors for intrapellet and bed diluent-to-catalyst mass ratios above 50 (SiO_2/catalyst) and 150 (quartz/catalyst), respectively. These data confirm that these dilution levels make local temperatures and concentrations at the catalyst sites identical to those in the extrapellet fluid phase; therefore, rates reported herein reflect the intrinsic chemical reaction rates devoid of transport artifacts. In the next sections, we examine the dependence of reactive CH_4 collision probabilities on O_2 pressures and the relative rates of CO and CH_4 reactions with chemisorbed O* intermediates.

3.2. Oxygen Selectivity in Reactions with CO and CH_4 on Pd Clusters. CH_4 conversion turnover rates and CO selectivities were measured on Pd/Al_2O_3 (0.2 wt % Pd, 21.3 nm mean cluster diameter) at 873 and 973 K during initial contact with CH_4–O_2 reactants (at times of 0–7.2 ks) (Figure 1). Reactive CH_4 collision probabilities (also denoted as first-order rate constants $\{r_{CH_4}(CH_4)^{-1}\}$) depend on O_2 pressures (Figure 1a,c); these trends are interpreted mechanistically in Sections 3.4 and 3.5. The effects of O_2 pressure on rate constants and their temporal evolution are similar on Pd clusters of different size (4.5–22.3 nm), in spite of the much larger rate constants measured on the larger clusters (to be discussed in Section 3.7). CO selectivities, reported as CO/(CO+CO_2) ratios in products, reached values as high as 0.9 after O_2 was depleted, but trace CO levels (<60 Pa CO) were detected only for outlet O_2 pressures below 0.01 kPa at 873 K (<22 Pa CO for <0.04 kPa O_2 at 973 K) (Figure 1b,d).

The maximum CO (or H_2) yields attainable from CH_4–O_2 mixture (defined as the ratio of CO outlet to CH_4 inlet molar concentrations and expressed in percentage, $\%Y_{CO}$) are determined by the reactivities of CO and CH_4 with O_2-derived chemisorbed species. The relative reactivities are given, in turn, by the ratio of reactive collision probabilities of CO and CH_4, which is defined here as the O* selectivity:

$$O^* \text{ selectivity} = \frac{r_{CO}(CO)^{-1}}{r_{CH_4}(CH_4)^{-1}} \qquad (1)$$

Scheme 1. Proposed Sequence of Elementary Reaction Steps for CH_4–O_2 Reactions on Supported Pd Clusters

	Elementary Step	Rate/ Equilibrium Constant
Step 1.1	$O_2(g) + * \rightleftarrows O_2*$	k_{1af}, k_{1ar}
Step 1.2	$O_2* + * \rightleftarrows 2O*$	k_{1bf}, k_{1br}
Step 2.1	$CH_4 + * + * \longrightarrow CH_3* + H*$	$k_{[*\text{-}*]}$
Step 2.2	$CH_4 + O* + * \longrightarrow CH_3* + OH*$	$k_{[O*\text{-}*]}$
Step 2.3	$CH_4 + O* + O* \longrightarrow CH_3O* + OH*$	$k_{[O*\text{-}O*]}$
Step 3	$C* + O* \rightleftarrows CO* + *$	k_{3f}, k_{3r}
Step 4	$CO* + O* \rightleftarrows CO_2* + *$	$k_{CO,f}, k_{CO,r}$
Step 5	$2OH* \overset{\circ}{\rightleftarrows} H_2O* + O*$	K_{OH*}
Step 6	$H_2O* \overset{\circ}{\rightleftarrows} H_2O + *$	K_{H_2O}
Step 7	$CO_2* \overset{\circ}{\rightleftarrows} CO_2 + *$	K_{CO_2}
Step 8	$CO* \overset{\circ}{\rightleftarrows} CO + *$	$1/K_{CO}$

*denotes a surface Pd atom; $\rightarrow$, $\rightleftarrows$, and $\overset{\circ}{\rightleftarrows}$ denote irreversible, reversible, and quasi-equilibrated steps, respectively; k_{if} and k_{ir} are the forward and reverse rate coefficients, respectively, and K_i are the equilibrium constants for the various steps (i denotes the individual steps 1.1 to 8).

This value reflects the reactivity of O* atoms toward CO, if formed via CO* desorption before subsequent oxidation, for sequential oxidation to form CO_2 during the time scale of a CH_4 turnover.

O* selectivities were measured using $^{13}CH_4$–^{12}CO–O_2 reactants on 0.2 wt % Pd/Al_2O_3 (21.3 nm mean Pd cluster diameter) at conditions that led to complete O_2 conversion (Figure 2; 973 K, 4.85 kPa $^{13}CH_4$, 0.81 kPa ^{12}CO, 0.081–0.36 kPa O_2). O* selectivities were much larger than unity and increased with increasing inlet O_2/CO ratios, indicating that ^{12}CO scavenges O* much more effectively than CH_4. The increase in O* selectivities with O_2/CO ratios reflects a preference for ^{12}CO over $^{13}CH_4$ oxidation in regions near the reactor inlet, where O_2 pressures are higher, and indicates that detectable CO concentrations are unlikely to be observed when O_2 is present at any point along the reactor. After O_2 depletion, $^{13}CH_4$ reacts with the O* species derived from $^{12}CO_2$, which is formed in ^{12}CO oxidation, to form isotopically mixed CO molecules via reforming routes involving C–H bond activation on exposed Pd site pairs (step 2.1, Scheme 1). It also reacts with the O* species derived from the total combustion products in $^{13}CH_4$–O_2 reactions. These additional reactions contribute to the reactive collision probabilities of $^{13}CH_4$ (with O*). Even with these additional contributions, reactive collision probabilities for $^{13}CH_4$ (0.9 to 1.3 mol O_2 (g-atom $Pd_{surface}$ kPa s)$^{-1}$) were much smaller than for ^{12}CO (32–1650 mol O_2 (g-atom $Pd_{surface}$ kPa s)$^{-1}$) at all O_2/CO ratios (0.064 to 2.6; Figure 2).

Next, we examine the mechanistic basis for the observed effects of O_2/CO ratios, which determine the O* coverages, on O* selectivities (Figure 2). The O* coverages are given by kinetic coupling between O* removal by reactions with CO (r_{CO}) and CH_4 (r_{CH_4}) and O* formation from O_2 dissociation (r_{O_2}). For O* species at pseudo-steady-state

$$r_{O_2} = \nu_{CO} r_{CO} + \nu_{CH_4} r_{CH_4} \qquad (2)$$

ν_{CO} and ν_{CH_4} are the respective O_2 stoichiometric coefficients (ν_{CO} = 0.5 and ν_{CH_4} = 1.5 for CH_4 conversion to CO and H_2O and ν_{CH_4} = 2.0 for CH_4 combustion). The large selectivity ratios observed (>35 for $O_2/CO > 0.064$, Figure 2) indicate that r_{CO} is much larger than r_{CH_4}. Together with rate and equilibrium constants in Scheme 1, these results give O* coverages as a function of O_2/CO ratio (derivation in Supporting Information, Section 1)

$$\frac{(O^*)}{(*)} \approx \frac{2k_{1bf}K_{O_2}}{k_{CO,f}K_{CO}}\frac{(O_2)}{(CO)} \tag{3}$$

K_{O_2} and K_{CO} are the equilibrium constants for adsorption of O_2 ($k_{1af}(k_{1ar})^{-1}$, step 1.1) and CO (reverse of step 8) and k_{1bf} and $k_{CO,f}$ are the rate constants for O_2 dissociation (step 1.2) and CO oxidation (step 4), respectively, as defined in Scheme 1. This equation, taken together with C—H bond dissociation steps that occur preferentially on the *—* site pairs (step 2.1, Scheme 1)[27] prevalent at low O* coverages,[19] leads to a linear dependence of O* selectivities on O_2/CO ratios

$$\text{O* selectivity} = 2\upsilon_{O^*}\frac{k_{1bf}K_{O_2}}{k_{[*-*]}}\frac{(O_2)}{(CO)} \tag{4}$$

where υ_{O^*} is the ratio of stoichiometric coefficients for O_2 reactions with CO and CH_4.[33] Eq 4 accurately describes all data in Figure 2 ($(2\upsilon_{O^*}k_{1bf}K_{O_2}(k_{[*-*]})^{-1}$=503). We infer that O* species, present at low coverages during catalysis, are not involved in the kinetically relevant C—H bond activation step, but act instead only to remove the products of initial C—H bond activation in subsequent steps, as also found for CH_4 oxidation on Pt clusters.[19] If O* species were used in the kinetically relevant C—H bond activation steps, ^{12}CO and $^{13}CH_4$ would compete for vicinal O* atoms, and O* selectivities would be independent of O* coverages or O_2/CO ratios and given by the ratio of rate constants for CO oxidation and C—H bond activation on O*—* site pairs ($\upsilon_{O^*}k_{CO,f}K_{CO}(k_{[O^*-*]})^{-1}$, derivation in the Supporting Information, Section 2). The linear dependence of O* selectivities on O_2/CO ratios (Figure 2) indicates that any CO that desorbs unreacted from partial oxidation stoichiometric mixtures ($O_2/CH_4 \approx 0.5$) would rapidly react at the high O* coverages and O_2/CO ratios prevalent near the reactor inlet, which favor CO oxidation over C—H bond activation steps.

These measured O* selectivities allow estimates of maximum CO yields ($\%Y_{CO}$) by using mole balances (expressed as CO (y_{CO}) and CH_4 (y_{CH_4}) mole fractions) in plug-flow reactor models and assuming that all CH_4 turnovers lead to CO desorption before oxidation to CO_2 (derivation in the Supporting Information, Section 3)

$$\%Y_{CO} = \left(\frac{y_{CO}}{y_{CH_4,0}}\right)_{max} \times 100\%$$
$$= \frac{1}{\alpha - 1}\left(\exp\left(-\frac{1}{\alpha - 1}\ln(\alpha)\right) - \exp\left(-\frac{1}{1-\left(\frac{1}{\alpha}\right)}\ln(\alpha)\right)\right) \tag{5}$$

$$\alpha = \left(\frac{k_{CO,f}K_{CO}}{k_{[*-*]}}\right) \tag{6}$$

These equations give 0.1 to 2.7% maximum CO yields for the range of O* selectivities measured in our experiments (36—1300;[34] Figure 2).

Higher CO yields from CH_4—O_2 reactants would require faster oxidation rates for CH_4 than CO, which become possible only at very low O* coverages. These O* coverages are, however, impractical for the reaction stoichiometries (O_2/CH_4 = 0.5) required for practical CH_4 conversions. The much higher reactivity of CO compared with CH_4 (Figure 2), as also found for Pt[19] and Rh[35] catalysts, at all practical O* coverages and O_2/CO ratios renders CO formation via direct partial oxidation pathways infeasible. The O* coverages and O* selectivities toward CO would be even higher with CH_4—O_2 than with CH_4—CO—O_2 reactants, because CH_4 is a much less effective O* scavenger than CO. These conclusions are consistent with the absence of detectable CO levels at all O_2 pressures above 0.04 kPa in the reactor effluent (Figure 1b,d).

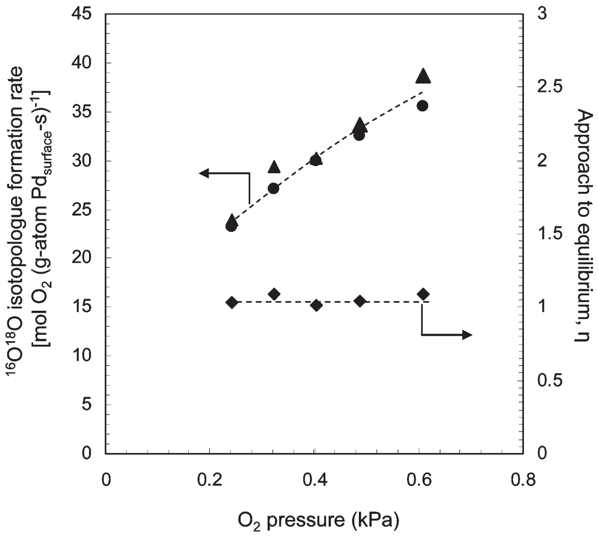

Figure 3. $^{16}O^{18}O$ isotopologue formation rates measured in $^{16}O_2$—$^{18}O_2$ (●) and CH_4—$^{16}O_2$—$^{18}O_2$ (▲) mixtures and the approach to equilibrium values {η(◆)}, which are the ratios of $^{16}O^{18}O$ isotopologue formation rates in CH_4—$^{16}O_2$—$^{18}O_2$ and $^{16}O_2$—$^{18}O_2$ mixtures, on a 0.2 wt % Pd/Al_2O_3 (21.3 nm mean Pd cluster diameter) catalyst at 873 K (▲: 4.86 kPa CH_4, 1.57 × 10^9 cm^3 (s g-atom $Pd_{surface}$)$^{-1}$, 200 SiO_2/catalyst intraparticle dilution ratio, 350 quartz/catalyst bed dilution ratio).

3.3. Chemical State of Pd Clusters during Catalytic CH_4—O_2 Reactions.

We probe next surface O* coverages on Pd clusters during CH_4—O_2 reactions and confirm that the bulk of Pd clusters remains in the metallic state throughout the rate measurements reported herein. During catalysis, surfaces of Pd clusters may not be equilibrated with O_2(g) because kinetic coupling between O_2 activation and its reactions with CH_4-derived intermediates can decrease O* coverages below those in equilibrium with O_2(g). Scavenging of O* by CH_4[19] or C_2H_6[36] reactants indeed prevents equilibration of O_2 dissociation—recombination steps on Pt.

$^{16}O^{18}O$ formation rates from $^{16}O_2$—$^{18}O_2$ mixtures in the presence and absence of CH_4 can establish the reversibility of O_2 dissociation steps (step 1, Scheme 1) and whether O* coverages are equilibrated with O_2(g) during catalysis. The ratio of $^{16}O^{18}O$ formation rates with CH_4—$^{16}O_2$—$^{18}O_2$ and $^{16}O_2$—$^{18}O_2$ mixtures (denoted as η) would be unity for equilibrated O_2 dissociation, but much smaller than unity for irreversible steps.[37] $^{16}O^{18}O$ formation rates were measured on Pd/Al_2O_3 (0.2 wt % Pd, 21.3 nm mean Pd cluster diameter) with and without CH_4 (4.86 kPa CH_4, 0.24 to 0.6 kPa O_2, 873 K, Figure 3) after reactions were conducted for >80 ks to achieve stable CH_4 conversion rates and first-order rate constants that are independent of O_2 pressure (Figure 1a). $^{16}O^{18}O$ isotopologue formation rates are proportional to $(O_2)^{1/2}$, suggesting that exchange involves reactions of O_2^* with O* on O*-saturated Pd clusters, as derived and shown experimentally.[20,37] $^{16}O^{18}O$ isotopologue formation rates for $CH_4-^{16}O_2-^{18}O_2$ and $^{16}O_2-^{18}O_2$ mixtures were the same within experimental accuracy at all O_2 pressures ($\eta = 1.01$ to 1.09; Figure 3), indicating that O* is equilibrated with O_2(g) during CH_4-O_2 reactions at these conditions. O* equilibration was also confirmed from CH_4 chemical conversion rates that consume O* atoms significantly lower than the O* recombination rates measured from oxygen isotopic exchange under all conditions during CH_4 oxidation catalysis on O* saturated surfaces (2.5 mol CH_4 (g-atom $Pd_{surface}$ s$)^{-1}$ versus 23−39 mol $^{16}O^{18}O$ (g-atom $Pd_{surface}$ s$)^{-1}$, 4.86 kPa CH_4, 873 K). We conclude that oxygen chemical potentials at Pd cluster surfaces during catalysis are equal to those in O_2(g) for all conditions used to measure the rate data reported in Sections 3.5−3.7 (873 K, <6 kPa CH_4, <1.6 kPa O_2). Therefore, equilibrium O_2 uptakes on Pd clusters (in the absence of CH_4) rigorously reflect the O* coverages during CH_4-O_2 reactions. These uptakes were measured at 873 K and 1−30 kPa O_2 on 2 wt % Pd/Al_2O_3 (5.9 nm mean Pd cluster diameter). Bulk oxidation of small Pd clusters has been shown to occur at lower oxygen chemical potentials than the large clusters used in the rate measurements reported herein (21.3 nm mean Pd cluster diameter).[29] The smaller Pd clusters (5.9 nm mean diameter) give constant oxygen uptakes, expressed in (O/Pd) atomic ratios, of 0.18 at O_2 pressures below 7.5 kPa. (See Figure S-1 in the Supporting Information Section 4 for the O_2 uptake as a function of O_2 pressure.) These ratios resemble those expected for saturation O* coverages (the expected O/Pd ratio is 0.17 for 5.9 nm hemispherical Pd clusters at surface saturation), as they correspond to an atomic ratio of oxygen-to-exposed Pd of 1.06. Above 7.5 kPa, the (O/Pd) ratios increased gradually from 0.18 and reached 0.98 at 25 kPa O_2. This increase corresponds to the formation of bulk PdO. These results confirm that small Pd clusters (5.9 nm), in spite of their stronger thermodynamic tendency for bulk oxidation,[29] retain their metallic bulk at temperatures (>873 K) and O_2 pressures (<1.6 kPa) used here. Larger metallic Pd clusters are expected to convert to PdO at even higher O_2 pressures; thus, Pd clusters of all diameters used in the rate measurements herein must also be in the metallic phase.[29]

Bulk oxidation of Pd clusters occurs at higher O_2 pressures and forms $Pd^{2+}-O^{2-}$ surface sites that are more effective than the O*−O* sites on metallic Pd clusters for C−H bond activation.[28] The Pd−PdO phase transition and its kinetic consequences in CH_4-O_2 reactions are addressed in a parallel study at thermodynamic and chemical equilibrium, where oxygen atoms at surfaces and in the bulk of Pd clusters are equilibrated with each other and with O_2(g).[29] Here, we specifically address the elementary steps and their kinetic relevance for CH_4 oxidation over O* covered metallic Pd clusters by keeping oxygen chemical potentials below those required for bulk oxidation (<7.5 kPa O_2, 873 K). We show that the reactive CH_4 collision probabilities depend on O* coverages in the same manner on Pd and Pt clusters, suggesting that identical kinetically relevant steps and surface site structures are involved and that they evolve with O* coverages in a similar manner.

Table 2. Reactive CH_4 Collision Probabilities ($r_{CH_4}(CH_4)^{-1}$, Also the First-Order Rate Constants) in CH_4-O_2 Mixtures and C−H Bond Activation Rate Constants on Metal Atom Site Pairs (Measured in CH_4-CO_2 or CH_4-H_2O Mixtures) on Pd Clusters at 873 and 973 K

reaction mixture	mean Pd cluster size	first-order rate constant (mol CH_4 (g-atom $Pd_{surface}$ s kPa$)^{-1}$)	
	(nm)	873 K	973 K
CH_4-O_2	21.3	34.6[a]	58.2[a]
CH_4-CO_2	12.5	4.0[b]	12.2[b]
CH_4-H_2O	12.5	4.3[b]	12.9[b]

[a] 0.2 wt % Pd/Al_2O_3, 0.17 kPa O_2, 3.6 ks time-on-stream, 1.57×10^9 cm^3 (s g-atom $Pd_{surface}$$)^{-1}$, 200 SiO_2/catalyst intraparticle dilution ratio, 450 quartz/catalyst bed dilution ratio. [b] 1.6 wt % Pd/ZrO_2 from ref,[27] see note in ref [38] for the effects of cluster size.

3.4. Reactive CH_4 Collision Probabilities on Pd Metal Clusters.

CH_4 conversion turnover rates were measured during initial contact (0−7.2 ks) of Pd/Al_2O_3 (0.2 wt %, 21.3 nm mean cluster diameter) with CH_4-O_2 reactants by varying O_2 pressures at a constant CH_4 pressure (4.85 kPa). Reactive CH_4 collision probabilities are shown in Figure 1a,c as a function of O_2 pressures at 873 and 973 K, respectively. The reactive CH_4 collision probabilities were constant at high O_2 pressures (>1.1 and >1.3 kPa for 873 and 973 K, respectively) but increased as O_2 pressure decreased, as also observed on Pt clusters.[20] These trends were interpreted from kinetic and isotopic data and density functional theory calculations on Pt clusters in terms of a transition in the identity of the kinetically relevant step and of the most abundant surface intermediate with changes in O* coverages.[20] Specifically, kinetically relevant C−H bond activation steps occur on O*−O* site pairs at high O* coverages but benefit from access to vacant sites in O*−* site pairs as O* coverages decrease with decreasing O_2 pressures. The vacant sites can interact with the C atom in CH_3 groups and stabilize C−H bond activation transition states, causing the observed increase in reactivity on Pd clusters as O_2 pressure decreases, as also found on Pt clusters.[20]

Reactive CH_4 collision probabilities did not depend on O_2 pressure above 1.1−1.3 kPa O_2 (Figure 1a,c), because kinetically relevant C−H bond activation step must use O*−O* site pairs on O*-saturated cluster surfaces, a conclusion confirmed by rate dependencies, normal CH_4/CD_4 kinetic isotope effects, and high C−H bond activation barriers and pre-exponential factors prevalent for O* assisted C−H bond activation steps, as discussed in Section 3.5. As vacant sites emerge with decreasing O_2 pressures, the first-order C−H bond activation rate constants increased and reached values larger than for similar steps on *−* site pairs,[38] which limit rates for CH_4-H_2O/CO_2 mixtures[27] (step 2.1, Scheme 1; Table 2). On Pt cluster surfaces of high O* coverages, O* atoms vicinal to exposed metal atoms activate C−H bonds during CH_4-O_2,[19] $C_2H_6-O_2$,[36] and $CH_3OCH_3-O_2$[39] reactions much more efficiently than metal atom site pairs. O* abstracts H atoms from CH_4, whereas exposed metal atoms stabilize CH_3 fragments via concerted oxidative addition into the C−H bond.[20] These O*−* site pairs are also more reactive than O*−O* site pairs on both Pd and Pt[20,36] surfaces because CH_3 fragments interact with open sites (*) more strongly than with O* and stabilize the required transition states. Taken together, the trends of first-order rate constants with O_2 pressures in Figure 1 suggest that O*−* site pairs assist C−H bond activation much more effectively than the *−* or O*−O* site pairs prevalent in

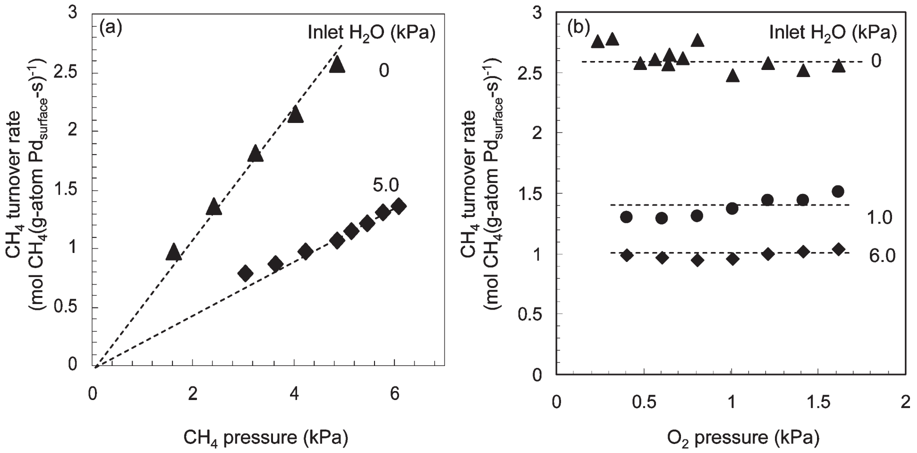

Figure 4. (a) Effects of CH_4 pressure on CH_4 turnover rates during CH_4−O_2 (▲, 0.48 kPa O_2) and CH_4−O_2−H_2O (◆, 0.48 kPa O_2 and 5.0 kPa H_2O) reactions at 873 K on a 0.2 wt % Pd/Al_2O_3 (21.3 nm mean Pd cluster diameter) catalyst. (b) Effects of O_2 pressure on CH_4 turnover rates during CH_4−O_2 reactions at 873 K on a 0.2 wt % Pd/Al_2O_3 (21.3 nm mean Pd cluster diameter) catalyst with CH_4−O_2−H_2O mixtures (4.86 kPa CH_4; ▲: 0 kPa H_2O; ●: 1.0 kPa H_2O; ◆: 6.0 kPa H_2O).

the absence of O_2 (in CH_4−H_2O/CO_2 mixtures) or at high O_2 pressures, respectively.

At very low O_2 pressures, O_2 activation becomes the kinetically relevant step on Pt clusters (8.5 nm mean cluster diameter, $O_2/CH_4 < 0.08$,[40] 873 K).[19] In this regime, turnover rates become proportional to O_2 pressure and independent of CH_4 pressure, and CH_4/CD_4 isotope effects are not detected. On Pd, this kinetic regime was detected only at high temperatures (973 K) and very low O_2 pressures (<0.2 kPa; Figure 1c). This difference between Pd and Pt reflects stronger O*−Pd bonds than O*−Pt bonds (382 vs 354 kJ mol^{-1} DFT calculated values of an isolated O* atom on Pd(111) and Pt(111) surfaces, respectively[41]), making bare surfaces essentially inaccessible before O_2 depletion and the regime that O_2 dissociation controls rates nearly undetected on Pd clusters.

The reactive CH_4 collision probabilities did not change with time on stream at extended times (similar at 32.4−38.0 and 77.4−82.8 ks; Figure 1a,c), but the rate constants and the transition O_2 pressure between regimes were smaller than those measured during initial contact to CH_4−O_2 reactants (0−7.2 ks). These changes appear to reflect the densification of O* monolayers, as proposed on Pd(100),[42,43] and the formation of more stable structures, within which oxygen vacancies (*) are less likely to exist. Therefore, turnover rates and rate constants become smaller after densification, and lower O_2 pressures are required for vacancies to form in concentrations for O*−* sites to contribute to C−H bond activation rates (<0.2 and <0.3 kPa for 873 and 973 K, respectively). These "deactivation" processes do not reflect the coalescence of Pd clusters because larger clusters would have led to lower O* binding energies and higher reactivity (Section 3.7) and to a transition between regimes to occur at higher O_2 pressures.

3.5. Rate Equations and Their Mechanistic Interpretations for CH_4−O_2 Reactions on Oxygen-Saturated Pd Cluster Surfaces. Next, we report kinetic effects of reactant and product concentrations and CH_4/CD_4 kinetic isotope effects at reaction times (>80 ks) and conditions that led to stable rates and to first-order rate constants independent of O_2 pressure on Pd/Al_2O_3 (0.2 wt %, 21.3 nm mean Pd cluster diameter) at low CH_4 conversions (<0.5%; H_2O and CO_2 <0.05 kPa at 873 K). CH_4 turnover rates (r_{CH_4}) increased linearly with CH_4 pressure (1.8−5 kPa) but did not depend on O_2 pressure (0.4−1.6 kPa; Figures 4a,b) according to the equation

$$r_{CH_4} = k_{app,1}(CH_4)^1(O_2)^0 \qquad (7)$$

in which $k_{app,1}$ is an effective rate constant. This equation describes the rate data on Pd clusters with mean cluster diameters between 4.5 and 22.3 nm.

These rate data (Figure 4) are consistent with the sequence of elementary steps shown in Scheme 1. In this mechanistic proposal, O_2 dissociates to form O* species (steps 1.1 and 1.2, Scheme 1), and the resulting O*−O* site pairs activate C−H bonds in CH_4 (step 2.3) to form CH_3O* and OH*. CH_3O* undergoes sequential H-abstraction and O* insertion (step 3) steps to form CO (step 8) or CO_2 (steps 4 and 7). OH* recombination forms H_2O (steps 5 and 6) and CO readsorption (reverse of step 8) and oxidation to CO_2 (steps 4 and 7) complete a catalytic turnover. O_2 dissociation steps (steps 1.1 and 1.2) are quasi-equilibrated, confirmed from equal $^{16}O^{18}O$ isotopologue formation rates measured during catalysis (in CH_4−$^{16}O_2$−$^{18}O_2$) and at oxygen chemical equilibrium (in $^{16}O_2$−$^{18}O_2$) and their rate ratios (η) of unity (Section 3.3). CH_4/CD_4 kinetic isotope effects, measured on the Pd/Al_2O_3 catalyst (0.2 wt %, 21.3 nm mean Pd cluster diameters) with CH_4−O_2 and CD_4−O_2 mixtures are 2.01 at 873 K; these values confirm that C−H bond activation is a kinetically relevant step; the linear dependence of rates on CH_4 pressure indicates that C−H bond activation occurs on surfaces with active site structures and concentrations that do not depend on the CH_4 or O_2 pressure. This requires that cluster surfaces be either uncovered or saturated by species derived from CH_4 or O_2 (CH_x* and O*, respectively).

Kinetic studies[27] with CH_4−H_2O/CO_2 reactants showed that C* intermediates are present in kinetically detectable coverages on Pd clusters because of strong Pd−C bonds, but such species do not influence CH_4−O_2 reactions because O_2 is a more effective oxidant than H_2O and CO_2, confirmed from larger CH_4 oxidation rates during reactions with O_2 than with H_2O and CO_2 (Table 2). Pd cluster surfaces partially covered with C* from C−H bond activation steps would have led to different $^{16}O^{18}O$ formation rates with CH_4−$^{16}O_2$−$^{18}O_2$ and $^{16}O_2$−$^{18}O_2$ mixtures, instead of the equal rates measured (Figure 3). Reactive CH_4 collision probabilities and the activation barriers and pre-exponential factors for C−H bond activation in CH_4 on

Table 3. Activation Barriers, Pre-Exponential Factors, and Activation Entropies for C−H Bond Activation on Oxygen Atom (O*−O*) and Metal Atom (*−*) Site Pairs on Pd and Pt Cluster Surfaces

metal (cluster size, nm)	site pair	reaction mixture	activation barrier (kJ mol^{-1})	pre-exponential factor (kPa^{-1} s^{-1})	activation entropy (J mol^{-1} K^{-1})[a]
Pd (21.3)[b]	O*−O*	CH_4−O_2	158	1.5×10^9	−12.6
Pd (12.5)[c]	*−*	CH_4−CO_2	84	4×10^5	−81.0
		CH_4−H_2O	81	3×10^5	−83.4
Pt (8.5)[b]	O*−O*	CH_4−O_2	155	2.1×10^9	−9.8

[a] Standard state 1 mol dm^{-3}. [b] 0.2 wt % Pd or Pt on Al_2O_3. [c] 1.6 wt % Pd/ZrO_2 from ref 27.

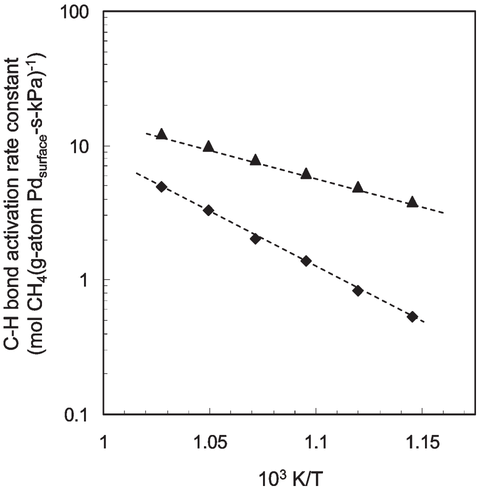

Figure 5. Arrhenius plot of C−H bond activation rate constants in CH_4−O_2 mixtures on Pd clusters (◆, 21.3 nm mean diameter; 0.2 wt % Pd/Al_2O_3) and C−H bond activation rate constants on *−* site pairs on Pd clusters (▲, 12.5 nm mean diameter, CH_4−CO_2/H_2O mixtures, from ref 27) (CH_4−O_2: 9.4×10^8 cm^3 (s g-atom Pd$_{surface}$)$^{-1}$, 200 SiO_2/catalyst intraparticle dilution ratio, 280 quartz/catalyst interparticle dilution ratio; CH_4−CO_2/H_2O: see ref 27 for reaction conditions).

uncovered Pd clusters (step 2.1, Scheme 1) have been previously established using CH_4−H_2O/CO_2 mixtures ($k_{[*-*]} \approx 4.0$ mol CH_4 (g-atom Pd$_{surface}$ kPa s)$^{-1}$ at 873 K; activation barrier 81−84 kJ mol^{-1}; pre-exponential factor (3−4) × 10^5 kPa^{-1} s^{-1}; 12.5 nm mean Pd cluster diameter; Table 3).[27,38] These values were unlike those measured in CH_4−O_2 reactions (0.53 mol CH_4 (g-atom Pd$_{surface}$ kPa s)$^{-1}$ at 873 K; activation barrier 158 kJ mol^{-1}; pre-exponential factor 1.5 × 10^9 kPa^{-1} s^{-1}; 21.3 nm mean Pd cluster diameter; Table 3), derived from regression fitting of the temperature dependence rate constant data in Figure 5. These distinct kinetic parameters led us to conclude that the active site structures in CH_4−O_2 and in CH_4−H_2O/CO_2 reactions must be different. In contrast with CH_4−H_2O/CO_2 reactions, Pd cluster surfaces were not uncovered in CH_4−O_2 reactions but instead saturated with O* atoms, a conclusion consistent with the atomic ratio of oxygen-to-exposed Pd (O*/Pd$_{surface}$) of near-unity (1.06) over the O_2 pressure range (0.5−6.0 kPa, Section 3.3), which determines the oxygen chemical potentials at Pd cluster surfaces used for rate measurements. (See Figure S-1 of the Supporting Information, Section 4.) The apparent rate constant in eq 7, $k_{app,1}$, thus reflects the elementary rate constant for C−H bond activation on O*−O* site pairs ($k_{[O^*-O^*]}$, step 2.3).

The activation energy (158 kJ mol^{-1}) and pre-exponential factor (1.5 × 10^9 kPa^{-1} s^{-1}) for C−H bond activation on O*−O* site pairs on Pd/Al_2O_3 (0.2 wt %, 21.3 nm clusters; Figure 5) are similar to those on Pt clusters (155 kJ mol^{-1} and 2.1 × 10^9 kPa^{-1} s^{-1}, 8.5 nm clusters).[20] These activation barriers are similar to DFT-derived C−H bond dissociation barriers on O* saturated Pt(111) (149 kJ mol^{-1})[20] and Pd(111) (145 kJ mol^{-1})[44] surfaces and on O* saturated surfaces of cuboctahedral Pt clusters (149 kJ mol^{-1}; 201 Pt atoms).[20] C−H bond activation on O*−O* site pairs involves H-atom abstraction by one O* to form a [CH_3•−O*−OH*]‡ transition state,[20,44] in which the O−H* bond is nearly formed and the CH_3• radical-like species interacts weakly with a vicinal O*, as also proposed for C−H bond activation on V-oxide.[45,46] These unstable CH_3 species lead to transition-state energies much higher than those on O*−* pairs, where CH_3 species interact strongly with the * at the transition state.[20] Weakly held CH_3• species retain most of the translational entropy of the CH_4 reactants. As a result, activation entropies are much less negative when O*−O* (−12.6 and −9.8 J (mol K)$^{-1}$ for Pd and Pt,[20] respectively) instead of O*−* pairs (−97.1 J (mol K)$^{-1}$ for Pt)[20] are used for C−H bond activation; their values are also much smaller (in negative values) than estimates by assuming the loss of one translational mode upon formation of the transition state from the gas phase CH_4 reactant in the framework of transition state theory (−96 J (mol K)$^{-1}$).

3.6. CO_2 and H_2O Effects on CH_4−O_2 Reaction Rates. Next, we consider the influences of excess CO_2 and H_2O products on CH_4 conversion turnover rates and their mechanistic implications. The kinetic consequences of excess H_2O and CO_2 were measured by adding H_2O and $^{12}CO_2$ to CH_4−O_2 (or $^{13}CH_4$−O_2) reactants. $^{13}CH_4$ turnover rates were not affected by $^{12}CO_2$ (6−12.5 kPa, Figure 6) because CO_2-derived intermediates (CO_2* and CO*) were present at negligible coverages during steady-state catalysis. CH_4 turnover rates decreased markedly when H_2O was added (1−10 kPa). Assumptions of competitive OH* adsorption via quasi-equilibrated H_2O adsorption−desorption steps (steps 5 and 6, Scheme 1), together with irreversible C−H bond activation on O*−O* site pairs and quasi-equilibrated O* adsorption−desorption steps, lead to the rate equation below (derivation in Supporting Information, Section 5):

$$r_{CH_4} = \frac{k_{[O^*-O^*]}(CH_4)K_{O_2}(O_2)}{\left(\sqrt{K_{O_2}(O_2)} + \sqrt{\dfrac{(H_2O)\sqrt{K_{O_2}(O_2)}}{K_{H_2O}K_{OH^*}}}\right)^2} \qquad (8)$$

This equation is used to describe the rate data in CH_4−O_2−H_2O mixtures (Figure 6) by linear regression analysis with minimization of residuals. Turnover rates decreased more strongly with increasing H_2O pressure than indicated by the functional form of eq 8 (Figure 6), and H_2O removal led to the partial recovery of

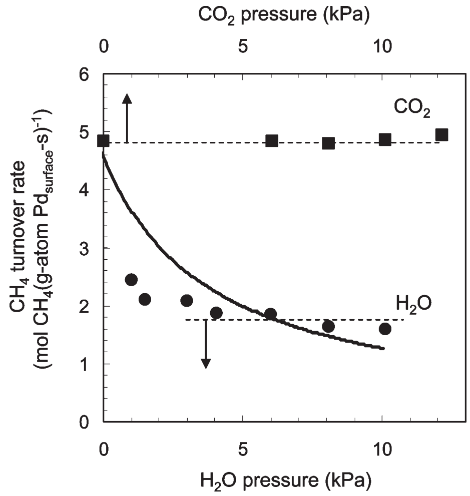

Figure 6. H_2O (●) and CO_2 (■) pressure effects on CH_4 turnover rates during $CH_4-O_2-H_2O$ (●) or $^{13}CH_4-O_2-CO_2$ (■) reactions on a 0.2 wt % Pd/Al_2O_3 (21.3 nm mean Pd cluster diameter) catalyst at 873 K. The solid line describes the fit from linear regression of rate data with a rate equation (eq 8) derived from assumptions of equilibrated H_2O and O_2 adsorption−desorption steps and irreversible C−H bond activation on O*−O* pairs ($CH_4-O_2-H_2O$ (●): 0.4 kPa O_2, 4.9 kPa CH_4; $^{13}CH_4-O_2-CO_2$ (■): 1.6 kPa O_2, 4.9 kPa CH_4; 1.57×10^9 cm^3 (s g-atom Pd$_{surface}$)$^{-1}$, 200 SiO_2/catalyst intraparticle dilution ratio, 450 quartz/catalyst interparticle dilution ratio).

initial turnover rates. These effects of H_2O and the incomplete recovery upon H_2O removal indicate that the decrease does not reflect kinetic inhibition processes caused by competitive adsorption. Turnover rates at concentrations much higher than those prevalent during catalysis H_2O (>5 kPa H_2O) remain proportional to CH_4 pressures (Figure 4a) and unaffected by O_2 pressures (Figure 4b), and thus C−H bond activation remains kinetically relevant and the number and identity of surface sites are insensitive to changes in O_2 pressure. These results suggest that Pd surfaces form structures that are more stable and less reactive in the presence of H_2O; such structures form catalytic sites that are unaffected by O_2 pressure and by further increase in H_2O pressure.

The involvement of OH* (or OD*) species in the kinetically relevant C−H bond dissociation step and the reversibility of this step can be probed in $CH_4-O_2-D_2O$ mixtures where OH* (or OD*) species are prevalent on Pd cluster surfaces. CH_3D must form via the microscopic reverse of the C−H bond activation steps (step 2.3, Scheme 1). The reversibility of this step is expressed in terms of the ratio of CH_xD_{4-x} formation to forward CH_4 conversion rates; these ratios were measured with $CH_4-O_2-D_2O$ and $CD_4-O_2-H_2O$ mixtures on 0.2 wt % Pd/Al_2O_3 (21.3 nm mean Pd cluster diameter) at 873 K, as shown in Figure 7, as a function of D_2O or H_2O inlet pressures (2−8 kPa). CH_3D (or CD_3H) isotopologues were the primary exchange product detected (>0.99 of all the CH_xD_{4-x}, $x = 0-3$) in $CH_4-D_2O-O_2$ (or $CD_4-H_2O-O_2$) mixtures, indicating that initial C−H bond activation is a reversible step in the presence of excess D_2O (or H_2O). The formation of these isotopologues infers the recombination of C−H (or C−D) bond dissociation products with OD* (or OH*) intermediates and, by microscopic reversibility, confirms that the initial C−H bond activation step involves O* and forms OD* (or OH*) species.

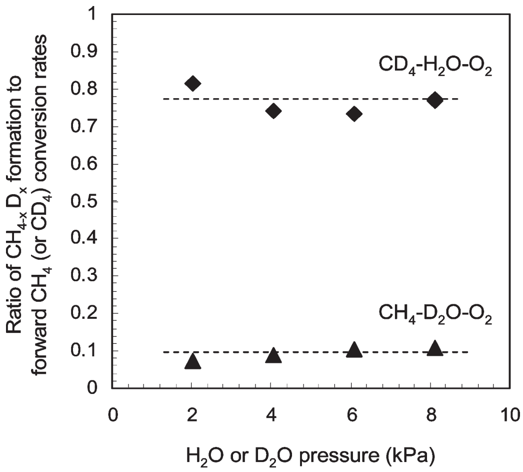

Figure 7. Ratio of CH_xD_{4-x} formation to forward CH_4 or CD_4 conversion rates in $CH_4-D_2O-O_2$ (▲) or $CD_4-H_2O-O_2$ (◆) mixtures at 873 K on a 0.2 wt % Pd/Al_2O_3 (21.3 nm mean Pd cluster diameter) catalyst (4.9 kPa CH_4 or CD_4, 1.6 kPa O_2, 2.35×10^8 cm^3 (s g-atom Pd$_{surface}$)$^{-1}$, 50 SiO_2/catalyst intraparticle dilution ratio, 350 quartz/catalyst interparticle dilution ratio).

The ratio of CH_3D formation to forward CH_4 conversion rates in $CH_4-D_2O-O_2$ (or $CD_4-H_2O-O_2$) mixtures reflects the relative rates of CH_3* (or CD_3*) and OD* (or OH*) recombination and forward CH_4 chemical turnover. These ratios were found to be 0.1 and 0.77 in $CH_4-D_2O-O_2$ and $CD_4-H_2O-O_2$ mixtures, respectively, and remain unchanged with D_2O (or H_2O) pressures (2−8 kPa), apparently because the active site structures on Pd cluster surfaces and OD* (or OH*) coverages do not vary with the D_2O (or H_2O) pressures, consistent with CH_4 turnover rates that remain essentially unaffected by D_2O (or H_2O) pressure at excess D_2O (or H_2O) (>4 kPa, Figure 6).

3.7. Effects of Pd Cluster Size and Oxygen Binding Strength on the Rates of C−H Bond Activation Assisted by Oxygen Atom Site Pairs. The average coordination of exposed metal atoms increases with increasing cluster size;[47] such an increase causes chemisorbed species to be more weakly bound on larger than smaller clusters. For CH_4-O_2 reactions on O*-covered surfaces, these weakly bound O* atoms would give higher turnover rates on larger clusters, a trend that we confirm from rate data on Pd clusters with 4.5−22.3 nm diameter in this section.

Rate constants for C−H bond activation on O*−O* site pairs ($k_{[O^*-O^*]}$) were measured in the early stages of reactions (0−7.2 ks) on Pd clusters (4.5−22.3 nm; 0.2 wt % Pd/Al_2O_3 catalysts) at 873 K (Figure 8). C−H bond activation rate constants increased markedly with increasing Pd cluster diameter (Figure 8), as also observed for CH_4-O_2[20] and $C_2H_6-O_2$[36] reactions on O* saturated Pt cluster surfaces. These trends reflect strong effects of oxygen binding energy on its reactivity for kinetically relevant H-abstraction steps and to a lesser extent its ability to weakly stabilize radical-like CH_3 fragments at the H-abstraction transition state (step 2.3, Scheme 1). On model Pt clusters, DFT-derived activation barriers for C−H bond dissociation on O*−O* site pairs decrease with decreasing O* binding energy and with increasing stability of OH*, which reflects, in turn, the O* basicity and the ability of O* to form stronger OH bonds at the transition states.

These effects of O* binding energy also cause differences in C−H bond activation reactivity between Pt and Pd atoms for a

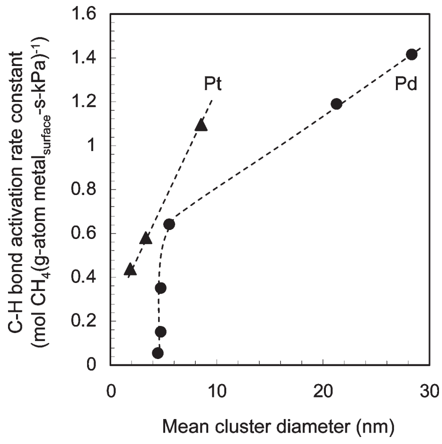

Figure 8. Cluster size dependence of initial rate constants for C—H bond activation on O*—O* site pairs on Pd (●) and Pt clusters (▲; from ref 20) at 873 K (●: 0.2 wt % Pd/Al_2O_3, 1.57 × 10^9 cm^3 (s g-atom $Pd_{surface}$)$^{-1}$, 200 SiO_2/catalyst intraparticle dilution ratio, 450 quartz/catalyst interparticle dilution ratio, measured within 7.2 ks after exposure to CH_4—O_2 feed mixtures; ▲: see ref 20 for specific reaction conditions for CH_4—O_2 reactions on 0.2 wt % Pt/Al_2O_3 catalysts).

given cluster size and average coordination. DFT-derived heats of atomic O* adsorption are 382 and 354 kJ mol^{-1} for isolated O* chemisorbed on the fcc sites of Pd(111) and Pt(111) surfaces, respectively.[41] The weakly bound O* on Pt are more effective for C—H bond activation than on Pd atoms and lead to higher turnover rates for Pt when compared at the same cluster size and average coordination (Figure 8).

When C—H bond activation occurs on O*—* site pairs, O* binding energy influences not only the O* reactivity but also the number of vacancies in O* monolayers; as a result, cluster size influences both turnover rates and the oxygen chemical potential at which O*—* sites become kinetically visible for the transition between kinetic regimes to occur. Figure 9 shows first-order rate constants (for 0—7.2 ks time on stream) as a function of O_2 pressure on samples with Pd clusters of 4.8 and 21.3 nm mean diameters (0.2 wt % Pd/Al_2O_3; 873 K). The reactivity of the small clusters is lower throughout this O_2 pressure range (0.3—1.6 kPa), although large and small clusters exhibit similar O_2 kinetic responses. The shift from O*—O* to O*—* as C—H bond activation sites, indicated by an increase in rate constants with decreasing O_2 pressure, occurs, however, at a lower O_2 pressure on small Pd clusters (~0.7 kPa on 4.8 nm; ~1.2 kPa on 21.3 nm). The stronger O* binding on small clusters leads to lower vacancy densities than that on large clusters at each O_2 pressure; as a result, contributions from the more reactive O*—* site pairs become kinetically visible only at lower O_2 pressures on the small clusters. These effects of cluster size on the involvement and reactivity of O*—* site pairs in C—H bond activation are similar to those observed for CH_4[20] and C_2H_6[36] oxidation on Pt and CH_3OCH_3 oxidation on Pt, Pd, and Rh.[48] The effects of surface coordination and cluster size on the binding energy of chemisorbed species and on the availability of vacancies are also evident from the lower reactivity of small clusters observed for NO oxidation on Pd,[37] for which rates are limited by O_2 activation on O*—* site pairs, and thiophene hydrodesulfurization on Ru[49] and Pt[50] clusters, for which rates depend on the availability of vacancies on cluster surfaces nearly saturated with chemisorbed sulfur atoms.

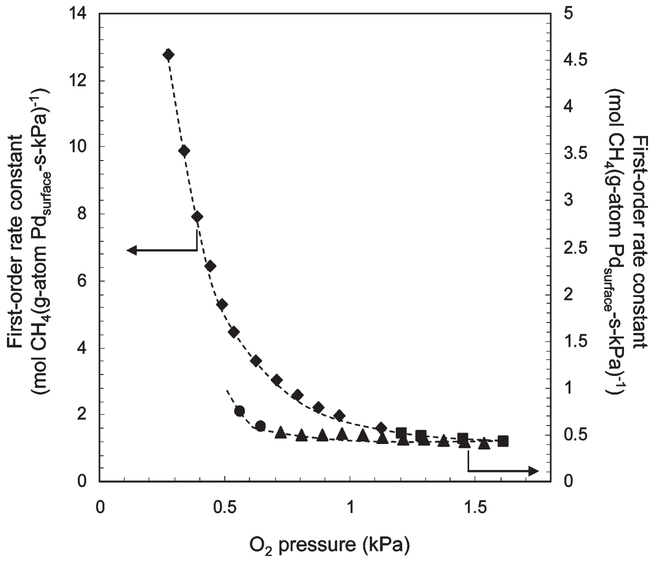

Figure 9. O_2 pressure effects on first-order rate constants (r_{CH_4}(CH_4)$^{-1}$) during CH_4—O_2 reactions on 0.2 wt % Pd/Al_2O_3 catalysts (4.8 (●,▲) and 21.3 nm (◆,■) mean Pd cluster diameters) at 873 K. Rate constants are inversely proportional to (◆,●) and independent of (■,▲) O_2 pressure (0—7.2 ks, 4.85 kPa CH_4, (1.31 to 1.57) × 10^9 cm^3 (g-atom $Pd_{surface}$ s)$^{-1}$, 200 SiO_2/catalyst intraparticle dilution ratio, 450 quartz/catalyst interparticle dilution ratio).

4. CONCLUSIONS

Elementary steps and their kinetic relevance during CH_4 reactions with O_2 on metallic Pd clusters were established based on kinetic and isotopic studies under conditions of strict kinetic control, attained by removal of temperature and concentration gradients within pellets and the catalyst bed by extensive site dilutions. H_2O and CO_2 were formed nearly exclusively at all nonzero O_2/CH_4 ratios because reactive collision probabilities for CO oxidation are much larger than those for CH_4 oxidation. This difference in reactivity between CO and CH_4 limits the maximum attainable CO yields from direct CH_4 and O_2 reactions at any practical extent of CH_4 conversion.

Reactive CH_4 collision probabilities (also the first-order rate constants) decrease and then reach constant values with increasing oxygen coverages. This trend reflects a transition in the kinetically relevant step from C—H bond activation on O*—* sites to less reactive O*—O* sites. The relative abundance of oxygen atoms and oxygen vacancies, distribution of O*—* and O*—O* pairs on Pd cluster surfaces, and thermodynamic tendency of bulk Pd oxidation during CH_4—O_2 reactions are set by the prevalent O_2 pressures because O* atoms and O_2(g) are chemically equilibrated. C—H bond activation step on O*—O* site pairs exhibits high barriers (158 kJ mol^{-1}) and unusually high pre-exponential factors (1.48 × 10^9 kPa^{-1} s^{-1}) that are larger than estimates derived from a transition-state theory formalism assuming the loss of a translational degree of freedom in CH_4(g). These kinetic parameters are common features for C—H bond activation on O* saturated metal surfaces, which proceeds via a loosely bound methyl radical-like transition state. In contrast, oxygen vacancies in O*—* site pairs stabilize the methyl group at the transition state, decreasing the barriers and, in turn, leading to more effective C—H bond activation on O*—* than O*—O* pairs.

Larger clusters with weakly bound O* are more effective for C—H bond activation than smaller clusters. The transition of kinetically relevant step from C−H bond activation on O*−* to O*−O* site pairs occurs at higher O_2 pressures on the larger Pd clusters because oxygen vacancies and O*−* pairs are more abundant than on the smaller clusters. Similar effects of O* binding strength are also observed among different metals. Stronger O* binding on Pd than Pt atoms of the same coordination leads to less effective C−H bond activation on the O*−O* pairs on Pd. These effects of O* binding strength on rates appear to be general for oxidation reactions that involve either the O* (CH_4 oxidation on Pd; CH_4, C_2H_6, and CH_3OCH_3 oxidation on Pt) or the oxygen vacancies (NO oxidation on Pt and Pd) in the kinetically relevant steps.

■ ASSOCIATED CONTENT

Ⓢ Supporting Information. Derivation of O*-to-* ratio in $^{13}CH_4$−^{12}CO−O_2 mixtures; derivation of O*-to-* ratio in $^{13}CH_4$−^{12}CO−O_2 mixtures assuming that C−H bond activation occurs on O*−* site pairs; estimation of maximum CO yields from oxygen selectivity values using mole balances in plug-flow reactor; equilibrium oxygen contents of Pd clusters (5.9 nm mean cluster diameter) at 873 K; derivation of rate expression for C−H bond activation on O*−O* site pairs on Pd surfaces nearly saturated with OH* species. This material is available free of charge via the Internet at http://pubs.acs.org.

■ AUTHOR INFORMATION

Corresponding Author

*E-mail: iglesia@berkeley.edu. Tel: (925) 323-5559.

■ ACKNOWLEDGMENT

This study was supported by BP as part of the Methane Conversion Cooperative Research Program. We thank Prof. Matthew Neurock and Drs. Corneliu Buda and Monica García-Diéguez for helpful technical discussions and their comments on the manuscript.

■ REFERENCES

(1) Ciuparu, D.; Lyubovsky, M. R.; Altman, E.; Pfefferle, L. D.; Datye, A. *Catal. Rev. Sci. Eng.* **2002**, *44*, 593.

(2) Chin, Y.-H.; Resasco, D. E. Catalytic Oxidation of Methane on Supported Palladium under Lean Conditions: Kinetics, Structure and Properties. In *Catalysis*; Spivey, J. J., Ed.; The Royal Society of Chemistry, Thomas Graham House, Science Park: Cambridge, U.K., 1999; Vol. 14, pp 1−39.

(3) Centi, G. *J. Mol. Catal. A: Chem.* **2001**, *173*, 287.

(4) Gelin, P.; Primet, M. *Appl. Catal., B* **2002**, *29*, 1.

(5) Claridge, J. B.; Green, M. L. H.; Tsang, S. C.; York, A. P. E.; Ashcroft, A. T.; Battle, P. D. *Catal. Lett.* **1993**, *22*, 299.

(6) Bhattacharya, A. K.; Breach, J. A.; Chand, S.; Ghorai, D. K.; Hartridge, A.; Keary, J.; Mallick, K. K. *Appl. Catal., A* **1992**, *80*, L1.

(7) van Looij, F.; Stobbe, E. R.; Geus, J. W. *Catal. Lett.* **1988**, *50*, 59.

(8) Armor, J. N. *Appl. Catal., A* **1999**, *176*, 159.

(9) Ribeiro, F. H.; Chow., M.; Dallabetta, R. A. *J. Catal.* **1994**, *146*, 537.

(10) McCarty, J. G. *Catal. Today* **1995**, *26*, 283.

(11) Hurtado, P.; Ordonez, S.; Sastre, H.; Diez, F. V. *Appl. Catal., B* **2004**, *51*, 229.

(12) Kimmerle, B.; Baiker, A.; Grunwaldt, J. D. *Phys. Chem. Chem. Phys.* **2010**, *12*, 2288.

(13) Matsumoto, H. *J. Phys. Chem.* **1994**, *98*, 5180.

(14) Matsumota, H.; Tanade, S. *J. Chem. Soc., Faraday Trans* **1994**, *90*, 3001.

(15) Datye, A. K.; Bravo, J.; Nelson, T. R.; Atanasova, P.; Lyubovsky, M.; Pfefferle, L. *Appl. Catal. A-Gen.* **2000**, *198*, 179.

(16) Farrauto, R. J.; Hobson, M. C.; Kennelly, T.; Waterman, E. M. *Appl. Catal., A* **1992**, *81*, 227.

(17) Farrauto, R. J.; Lampert, J. K.; Hobson, M. C.; Waterman, E. M. *Appl. Catal., B* **1995**, *6*, 263.

(18) Zhu, G.; Han, H.; Zemlyanov, D. Y.; Ribeiro, F. H. *J. Phys. Chem. B* **2005**, *109*, 2331.

(19) Chin, Y.-H.; Buda, C.; Neurock, M.; Iglesia, E. *J. Catal.* **2011**, doi:10.1016/j.jcat.2011.06.011.

(20) Chin, Y.-H.; Buda, C.; Neurock, M.; Iglesia, E. *J. Am. Chem. Soc.* **2011**, in press.

(21) Wei, J. M.; Iglesia, E. *J. Catal.* **2004**, *225*, 116.

(22) Wei, J. M.; Iglesia, E. *J. Phys. Chem. B* **2004**, *108*, 4094.

(23) Wei, J. M.; Iglesia, E. *J. Phys. Chem. B* **2004**, *108*, 7253.

(24) Wei, J.; Iglesia, E. *Phys. Chem. Chem. Phys.* **2004**, *6*, 3754.

(25) Wei, J.; Iglesia, E. *Angew. Chem., Int. Ed.* **2004**, *43*, 3685.

(26) Wei, J.; Iglesia, E. *J. Catal.* **2004**, *224*, 370.

(27) Yamaguchi, A; Iglesia, E. *J. Catal.* **2010**, *274*, 52.

(28) Chin, Y.-H.; Buda, C.; Neurock, M.; Iglesia, E. *J. Am. Chem. Soc.* in preparation.

(29) Chin, Y.-H.; García-Diéguez, M.; Iglesia, E., in preparation.

(30) David, R. L. *Handbook of Chemistry and Physics*, 87th ed.; CRC Press: Boca Raton, FL, 2006.

(31) Koros, R. M.; Nowak, E. J. *Chem. Eng. Sci.* **1967**, *22*, 470.

(32) Madon, R.; Boudart, M. *Ind. Eng. Chem. Fundam.* **1982**, *21*, 438.

(33) In $^{13}CH_4$-CO-O_2 mixtures and under the complete O_2 depletion, CH_4 can convert to CO_2 and CO with different reaction stoichiometries of O* atoms.

(34) The calculations assume that both CO and CH_4 oxidation reactions follow the first-order reaction kinetics.

(35) Donazzi, A.; Beretta, A.; Groppi, G.; Forzatti, P. *J. Catal.* **2008**, *255*, 241.

(36) García-Diéguez, M.; Chin, Y.-H.; Iglesia, E. *J. Catal.* **2011**, submitted.

(37) Weiss, B. M.; Iglesia, E. *J. Catal.* **2010**, *272*, 74.

(38) Elementary rate constants for C−H bond activation on *−* site pairs (step 2.1, Scheme 1) on the 21.3 nm Pd clusters are expected to be lower than the reported values on smaller Pd clusters in ref 27 because the metal sites with larger coordination are less effective for C-H bond activation (see refs 21−24, 26, and 27).

(39) Ishikawa, A.; Neurock, M.; Iglesia, E. *J. Am. Chem. Soc.* **2007**, *129*, 13201.

(40) On Pt clusters, this kinetic regime is defined by the O_2/CH_4 ratio because the O_2/CH_4 ratio determines the surface O* coverage via kinetic coupling of C−H and O═O activation steps.

(41) van Santen, R. A.; Neurock, M. *Molecular Heterogeneous Catalysis: A Conceptual and Computational Approach*; Wiley-VCH: Weinheim, Germany, 2006; p 107.

(42) Zheng, G.; Altman, E. I. *Surf. Sci.* **2002**, *504*, 253.

(43) Simmons, G. W.; Wang, Y.-N.; Marcos, J.; Klier, K. *J. Phys. Chem.* **1991**, *95*, 4522.

(44) Buda, C.; Neurock M., unpublished results.

(45) Dai, G.-L.; Liu, Z.-P.; Wang, W.-N.; Lu, J.; Fan, K.-N. *J. Phys. Chem. C* **2008**, *112*, 3719.

(46) Rozanska, X.; Fortrie, R.; Sauer, J. *J. Phys. Chem. C* **2007**, *111*, 6041.

(47) van Hardeveld, R.; Hartog, F. *Surf. Sci.* **1969**, *15*, 189.

(48) Ishikawa, A.; Iglesia, E. *J. Catal.* **2007**, *252*, 49.

(49) Wang, H.; Iglesia, E. *J. Catal.* **2010**, *273*, 245.

(50) Wang, H.; Iglesia, E. *ChemCatChem* **2011**, 3, 1166–1175.